Appl. Phys. B 81, 769–777 (2005)
DOI: 10.1007/s00340-005-1965-4

Applied Physics B
Lasers and Optics

G. WYSOCKI[1,✉]
R.F. CURL[1]
F.K. TITTEL[1]
R. MAULINI[2]
J.M. BULLIARD[2]
J. FAIST[2]

Widely tunable mode-hop free external cavity quantum cascade laser for high resolution spectroscopic applications

[1] Rice Quantum Institute, Rice University, 6100 Main St., Houston, TX 77005, USA
[2] Institute of Physics, University of Neuchâtel, 1 A.-L. Breguet, 2000 Neuchâtel, Switzerland

Received: 27 July 2005
Published online: 28 September 2005 •

ABSTRACT An external cavity (EC) quantum cascade laser (QCL) configuration with the thermoelectrically cooled gain medium fabricated using a bound-to-continuum design and operating in continuous wave at $\sim 5.2\,\mu$m is reported. The EC architecture employs a piezo-activated cavity mode tracking system for mode-hop free operation suitable for high resolution spectroscopic applications and multiple species trace-gas detection. The performance of the EC-QCL exhibits coarse single mode tuning over 35 cm^{-1} and a continuous mode-hop free fine tuning range of $\sim 1.2\,cm^{-1}$.

PACS 07.07.Df; 42.55.Px; 42.62.Fi; 42.60.Fc

1 Introduction

The development of laser spectroscopic techniques strongly relies on increasing the availability of new tunable laser sources. For applications in the mid-infrared (mid-IR) molecular fingerprint region, quantum cascade lasers (QCLs) have proved to be convenient and reliable light sources for the spectroscopic detection of trace gases [1–3, and references therein]. Spectroscopic applications usually require single mode operation. This is usually achieved by introducing a distributed feedback (DFB) structure into the QCL active region [4]. Although DFB QCLs show high performance and reliability, the range of wavelength tuning of the emitted laser radiation is limited by the limited tuning range of the DFB structures. Typically the maximum thermal tuning range of DFB-QCLs is of $\sim 10\,cm^{-1}$ [1, 2] achieved by varying either the temperature of the chip or the laser injection current. One of the disadvantages of such a thermal tuning is that it affects the effective gain of the QCL, which consequently causes a decrease of the output laser power with increasing temperature of the QCL chip.

In stark contrast, diode lasers in the visible and near-infrared that are tunable well over $200\,cm^{-1}$ have been developed and are commercially available as single frequency light sources for a wide range of spectroscopic applications [5]. The features that have made this possible, are a broad gain curve and the ability to operate in an external cavity (EC) configuration [6, 7]. The intrinsically broad gain curve of the diode laser arises because the curvatures of conduction and valence band of an energy versus k plot are always in opposite directions. Since the change in k upon photon emission is negligible, this means that photon energy changes rapidly with k so that broad gain results, even though conduction band momentum distributions are near thermal. For intersubband QC lasers, the curvatures are in the same direction and essentially match resulting in typically narrow gain profiles. However, as stated below, there exist schemes for broadening the gain profile of intersubband QC lasers.

High quality AR coatings in visible and near-IR wavelength range [5–7] or tilted diode laser output facets [8] result in an efficient reduction of the gain chip cavity finesse and enable mode-hop free wavelength tuning. These diode lasers operate at room temperature, but until recently QC lasers had to be operated well below room temperature often at cryogenic temperatures. In the mid-IR, AR coatings must be thicker because the wavelength is several times longer. It is very difficult to find an AR coating material of the right refractive index and optical properties that also has close to the same thermal expansion coefficient as the laser substrates. As a result, upon thermal cycling the AR coating tends to flake off. These two factors, intrinsically narrower gain curve and the need for lower temperature operation, have made the development of widely tunable mode-hop free laser sources for this spectral range challenging [9]. It should be noted here that other approaches can obviate the need for an AR coating e.g. an approach employing an integrated off-band surface emitting Bragg grating coupler which is currently under development [10]. This is a welcome and important development as near room temperature operation of QC lasers at long wavelengths presents an extremely formidable challenge.

Recently several groups have reported progress in the development of continuous wave (cw) QCLs operating at temperatures accessible with thermoelectric cooling [11–14], which significantly reduces the problem of AR coating degradation by thermal cycling. In particular the development of bound-to-continuum QC lasers [15] has greatly alleviated both of these impediments to wide frequency tuning. Bound-to-continuum QC lasers have an intrinsically broader gain profile because the lower state of the laser transition is a relatively broad continuum. A luminescence spectrum of

✉ Fax: 713 348 5686, E-mail: gerardw@rice.edu

297 cm^{-1} FWHM (full width at half maximum) at room temperature was observed for $\lambda \approx 10\,\mu m$ QCL devices employing bound-to-continuum transitions [16]. In addition, after an electron is driven to a particular continuum energy by stimulated emission, it is immediately relaxed over the continuum energies by phonon scattering. In other words, the lower state is a true continuum. As a result, competition by absorption from the lower state of the laser transition is virtually eliminated. This makes room temperature or near room temperature operation of the laser feasible. As a consequence, flaking of the AR coating by thermal cycling is eliminated. To take advantage of the broadband gain of such QCLs, an external cavity (EC) configuration can be used for wavelength selection [16–18].

Exploiting this development, this work reports on the development of a QC laser spectrometer for high resolution spectroscopic applications and multi species trace-gas detection in the mid-IR through the design and implementation of a novel EC-QCL architecture. The instrument employs a piezo-activated cavity mode tracking system for mode-hop free operation. The mode-tracking system provides independent control of the EC length and diffraction grating angle. The flexibility of this arrangement allows the instrument to be used with other QC lasers at other wavelengths without changing the EC configuration. System performance and spectroscopic application capability is demonstrated with a gain medium fabricated using a bound-to-continuum design and operating at $\sim 5.2\,\mu m$.

2 EC-QCL system configuration

The optical configuration of the EC-QCL, an upgraded version of a device first reported by Maulini et al. [17], is schematically shown in Fig. 1. The Littrow type EC arrangement consist of three main elements: the QCL chip, a beam collimating lens (24 mm-diameter $f/0.6$ germanium aspheric lens with a 3–12 μm AR coating), and a diffraction grating (150 grooves/mm blazed for a wavelength of 5.4 μm). The first order diffraction from the grating reflected with an efficiency of $\sim 95\%$ provides the laser feedback, while the zeroth order reflection provides the output laser beam.

The grating, GR, is mounted on the moving platform, which allows independent control of the EC length and grating angle. The platform position is controlled by a piezo-actuated linear translation stage (Physik Instrumente, model: M-014.00 and a piezo actuator model: P-840.60) as well as a rotary stage (Physik Instrumente, model: M-035.DP1), which is equipped with a motorized coarse angle control and piezo-actuated fine control. The applied components allow precise positioning of the EC length and grating angle with a resolution of < 0.9 nm and 1 μrad for external cavity length and grating angle respectively. The total greting angle range provided by PZT scanner is ±520 μrad. The coarse tuning by the linear motor can be performed within a range of ±6.3° and unidirectional repeatability of 10 μrad with the actual position measured by a built-in encoder with a resolution of $\sim 1.4\,\mu rad$/unit. The piezo-actuator controlling the external cavity length provides a total travel range of 90 μm ±20%, which can deliver a maximum continuous laser frequency tuning range of $\sim 2\,cm^{-1}$ (at $\lambda = 5\,\mu m$). The mirror, M, which is mounted together with the grating on the same platform, assures the same direction of the output EC-QCL beam.

The complete spectrometer depicted in Fig. 1 consists of two laser beam paths, which can be alternated by introducing a movable mirror, RM, into the optical axis. One optical arm includes a 1/8 m monochromator for coarse wavelength measurements. The other arm is used for spectroscopic absorption measurements or for relative and absolute spectral frequency standards such as a gas reference absorption cell or an air spaced etalon.

The gain chip used in the EC QCL was fabricated using a bound-to-continuum design applying essentially the same

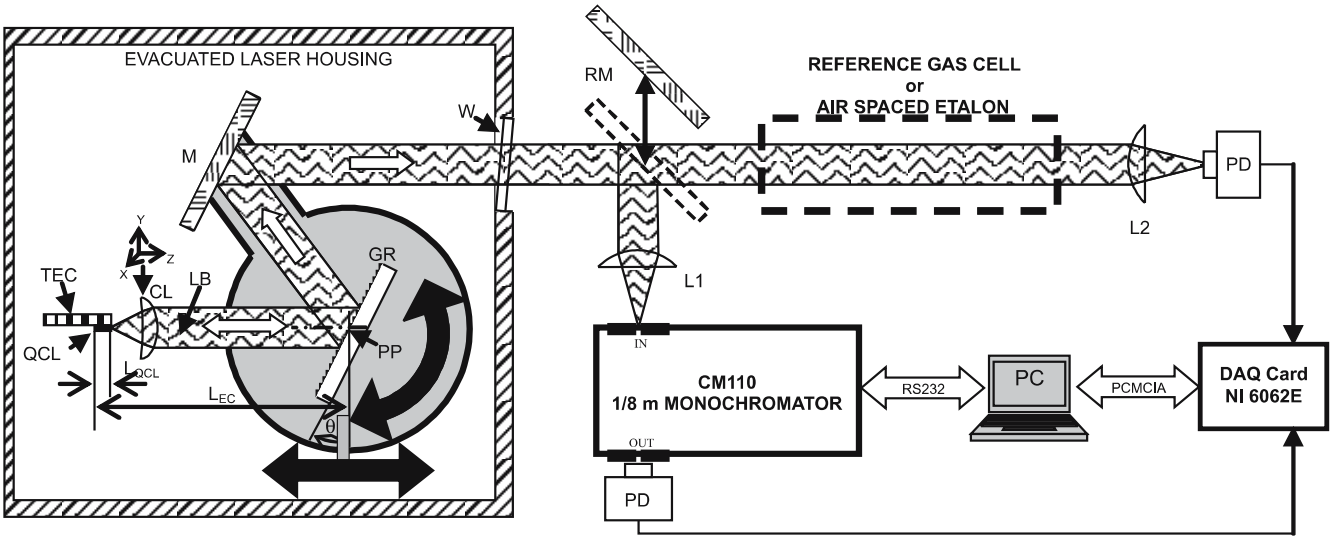

FIGURE 1 Schematic diagram of the EC QCL laser and the associated measurement system. QCL – quantum cascade laser, TEC – thermoelectric cooler, CL –collimating lens (1" diameter, $f/0.6$, Ge AR-coated 3–12 μm) mounted on a motorized 3D translation stage, LB –laser beam, GR – diffraction grating (150 gr/mm blazed for 5.4 μm), PP – pivot point of the rotational movement, M – mirror (mounted on the same platform with GR), W – CaF_2 window (thickness 4 mm, tilted $\sim 5°$), RM – removable mirror, PD –photodetector (Hg-Cd-Zn-Te, TE-cooled, Vigo Systems, PDI-2TE-6), L1, L2 – ZnSe lenses

processing methods and parameters as reported in [17]. A high-reflection (HR) coating (Al_2O_3/Au 300 nm/100 nm) was deposited on the back facet and an anti-reflection (AR) coating ($\lambda/4$ thick Al_2O_3 layer) was deposited on the front facet of the chip.

The AR coating is only partially necessary. In the center of the gain curve the reported EC-QCL configuration could operate without an AR coating applied to the front facet. However, the single frequency tunability of the EC QCL system will be strongly limited for both the fine wavelength tuning and the total wavelength range accessible by coarse tuning. Since the wavelength tuning is associated with the laser current scan, the range of laser current I_{QCL} available for a single mode scan can be approximated by the condition $I_{thEC} < I_{QCL} < I_{thQCL}$. Above I_{thQCL} the feedback from the QCL front facet reflection will be high enough to assure lasing conditions for the most favorable FP chip modes causing the laser to operate on hole burning modes near the highest gain as well as at the desired frequency.

Figure 2 shows the optical power of the QCL chip at $-30\,^{\circ}C$ and $-20\,^{\circ}C$ as a function of injection current measured at different stages of the chip fabrication. The characteristic threshold currents densities for the current chip operated at $-30\,^{\circ}C$ are : $J_{th(UC)} = 1.78\,kA/cm^2$, $J_{th(HR)} = 1.47\,kA/cm^2$, $J_{th(HR+AR)} = 2.37\,kA/cm^2$, $J_{th(EC)} = 1.93\,kA/cm^2$ for an uncoated chip, a HR coated back facet (value estimated for this temperature), an HR and AR coated chip and with EC feedback, respectively. These current densities allow the waveguide losses to be estimated as $\alpha_w \approx 7\,cm^{-1}$ and the total EC optical feedback to be estimated as $\sim 17\%$. The AR coating reflectance can be calculated as $\sim 1\%$. However because the threshold current density $J_{th(HR+AR)}$ was measured for a laser working in a strongly saturated regime close to power rollover, this value is only a rough estimate. Therefore for further calculations we will assume the AR coating reflectance to be at the level of 3%, which is a more typical value for such lasers (a similar value was measured in [17] for a similar device). Frequency measurements within the tuning range of the EC-QCL obtained with the 1/8 m monochromator are plotted in Fig. 3 for several positions of the diffraction grating together with a corresponding optical power measured at the laser output. The higher α_w and threshold current densities values (see the threshold current condition above) of the present gain medium, with respect to the QCL used in the previous version, result in a decrease in the achievable optical power and limit both the maximum tuning range of the EC-QCL system to $\sim 35\,cm^{-1}$ and the fine mode-hope free tuning range to $\sim 1.2\,cm^{-1}$. However, the parameters of the QCL gain chip are excellent for demonstrating the high resolution wavelength tuning capabilities of the EC-QCL employing the laser longitudinal mode tracking system.

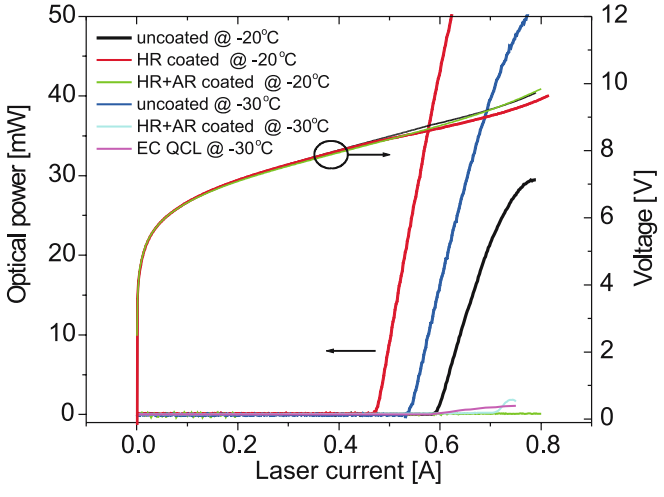

FIGURE 2 QCL I–V curves

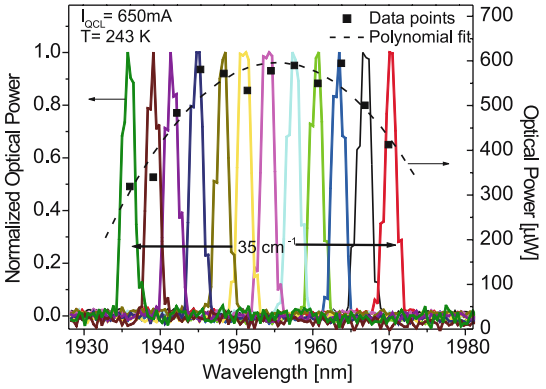

FIGURE 3 Wavelength tuning range of the EC-QCL measured with a 1/8 m monochromator together with the corresponding optical power

3 Wavelength tuning of the EC-QCL

3.1 *System simulation*

The complete laser cavity can be analyzed as a system of two coupled cavities: the QCL chip cavity between back and front facet of the QCL and the external cavity which consist of the HR coated back facet and the diffraction grating. The optical length of the QCL cavity is $L_{QCL} = n_{CKL} \times l \approx 1$ cm where n_{QCL} is a refractive index of the chip material and l is its length. The average optical length of the external cavity is ~ 9.3 cm. This results in free spectral range (FSR) of $0.5\,cm^{-1}$ (15 GHz) for the QCL. The EC Fabry–Pérot (FP) resonator has an FSR of $0.053\,cm^{-1}$ (1.6 GHz).

The diffraction grating acts as a band pass filter, for which the bandwidth can be estimated by calculating its resolving power

$$\Delta\lambda = \frac{\lambda}{|m|N} = \frac{\lambda d \cos\theta}{a}, \tag{1}$$

where λ represents the wavelength, $m = 1$ is a diffraction order, N is the number of grating lines illuminated, a is a diameter of the collimated laser beam and θ is the incident angle of the beam measured between the grating normal and the optical axis of the beam. For our system, where $\lambda = 5.2\,\mu m$, $d = 6.67\,\mu m$, $a =\sim 20$ mm and $\theta = 22.95°$ the approximation yields $\Delta\lambda =\sim 1.6$ nm ($\sim 0.6\,cm^1$, ~ 17.7 GHz).

The EC laser behavior during the frequency tuning process can be estimated by analyzing an optical system, which consist of two coupled optical cavities and the grating filter as discussed above. A block diagram of such a system is shown

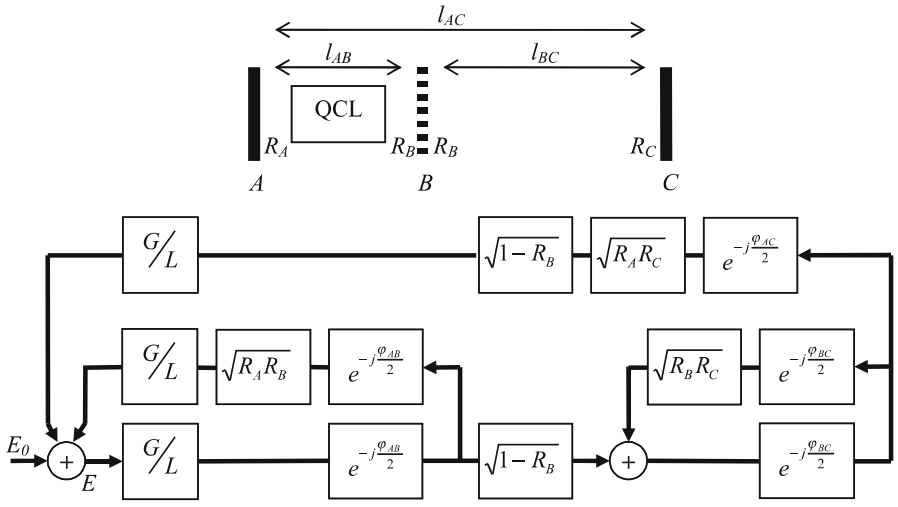

FIGURE 4 Block diagram of the model of an EC laser system with two coupled cavities

in Fig. 4. This yields an expression for the electric field in the QCL FP resonator:

$$E = E_0 \frac{1 - \sqrt{R_B R_C}\mathrm{e}^{-j\varphi_{BC}}}{\left(1 - \sqrt{R_B R_C}\mathrm{e}^{-j\varphi_{BC}} - \frac{G}{L}\sqrt{R_A R_B}\mathrm{e}^{-j\varphi_{AB}} - \frac{G}{L}\sqrt{R_A R_C}(1-2R_B)\mathrm{e}^{-j\varphi_{AC}}\right)},$$
$$\varphi = \frac{4\pi l}{\lambda}, \tag{2}$$

where c is velocity of light, λ represents the wavelength, R_A, R_B, R_C are the intensity reflection coefficients (reflectance) of the mirrors, φ_{AC}, φ_{AB}, φ_{BC} represent the phase shift during a single round trip between mirrors separated by distance l for the following pairs: A and C, A and B, and B and C respectively. $G(v) = \exp\left(\frac{1}{2}\gamma(v)l_{\mathrm{QCL}}\right)$ is the single pass gain coefficient and $L(v) = \exp\left(-\frac{1}{2}\alpha(v)l_{\mathrm{QCL}}\right)$ represent single pass waveguide losses. The presence of the grating can be simulated by substituting a reflectance of the external mirror by a grating reflectance function with a peak reflectance equal to R_C. For this estimation, the collimated laser beam can be approximated by an incident plane wave with intensity I_I illuminating N grooves of the grating. Since the grating does not introduce any phase shift for the incident wave, its wave reflection coefficient $\sqrt{R_{GR}}$ can be calculated using the intensity distribution of light reflected from the diffraction grating, which can be written as

$$\sqrt{R_{GR}} = \sqrt{\frac{I_R}{I_I}} = \frac{\sqrt{R_C}}{N}\left|\frac{\sin(N\phi/2)}{\sin(\phi/2)}\right|, \tag{3}$$

where I_R, is the total reflected intensity of light and φ is a phase difference between two partial waves reflected by neighboring grooves. For a diffraction grating mounted at an angle θ using a Littrow configuration, the phase difference can be expressed as $\phi = \frac{4\pi d}{\lambda}\sin\theta$, where d is a distance between two adjacent grooves.

The relative change in the intensity as a function of optical frequency calculated between mirrors A and B for a passive QCL FP resonator (assuming that QCL is transparent when $G = L$) and all frequency tuning elements (QCL and EC passive FP resonator modes and grating reflectivity spectrum) centered at the same wavelength is depicted in Fig. 5. The

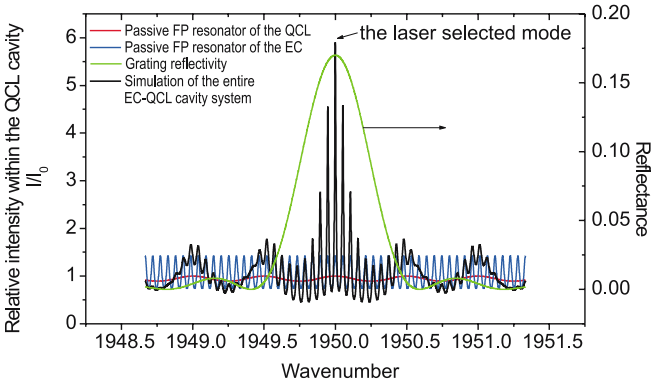

FIGURE 5 Numerical simulation of the relative change in the optical intensity between mirrors A and B as a function of optical frequency for the EC-QCL coupled cavity system calculated with an assumption of transparent QCL medium $G = L$ and for all frequency tuning elements (QCL and EC FP resonator modes and grating reflectance spectral characteristics) centered at the same wavelength

QCL is considered to be a homogenously broadened gain medium as the relaxation processes are fast. However, in the absence of any wavelength selecting element there are modes that have a spatial electric field distribution of their standing waves only weakly overlapped with the main longitudinal mode. These can simultaneously lase because of spatial hole burning. This is not the case for an EC grating coupled laser, where the separation of the EC FP modes selected by the grating is very small and the aforementioned spatial hole burning can not occur. In such a case, only the strongest of the grating selected longitudinal modes, for which also the phase condition is fulfilled, will lase. In other words, the laser will operate at the frequency of the highest overall peak and nowhere else.

Assuming the above, it is possible to simulate the tuning behavior of the laser, which can be done for four different situations:

1. tuning of the QCL cavity length while keeping the grating angle and its position with respect to the laser chip constant
2. simultaneous tuning of both the QCL cavity length and EC length while maintaining a constant grating angle

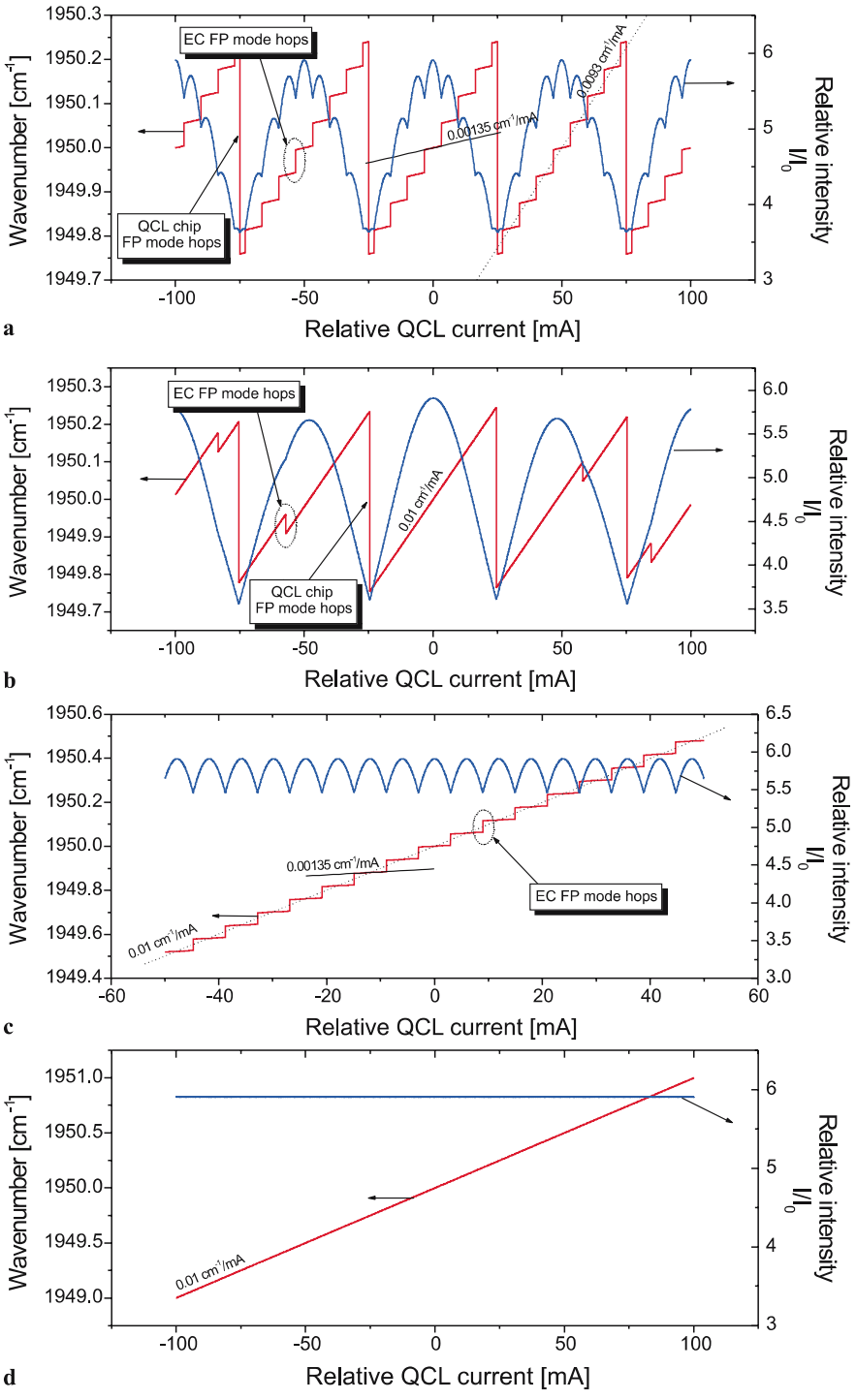

FIGURE 6 Results of the QCL FP resonator length scan simulation showing an optical frequency of the strongest longitudinal mode and its relative intensity for (**a**) no mode tracking, (**b**) mode tracking only with the EC length, (**c**) mode tracking only with grating angle and (**d**) mode tracking with all wavelength tuning elements. (The x scale shows optical frequency detuning from the state depicted in Fig. 5, which is expressed as a relative QCL current change calculated using experimentally measured coefficients)

3. simultaneous tuning of QCL cavity length and grating angle while keeping an EC length constant
4. simultaneous tuning of all three wavelength selective elements (i.e. QCL, EC length and grating angle)

The results of the simulation, which show the variations in the relative intensity and optical frequency of the most favorable mode, are shown in Fig. 6a, b, c, and d, respectively. In a real system, QCL cavity length tuning is actually caused by changes in the refractive index of the material due to modulation of carrier density generated by the injection current. The optical frequency tuning of the laser chip FP resonator measured when the QCL was operated in the middle of the gain curve (at $\sim 5.11\,\mu$m) and at an injection current of 650 mA, was found to be linear with a rate of $\frac{\mathrm{d}\nu}{\mathrm{d}I} \cong 0.01\,\frac{\mathrm{cm}^{-1}}{\mathrm{mA}}$. This value was used in the simulation. Since the QCL chip is also a part of the EC, the tuning rate of the EC FP modes at this wavelength should show a tuning rate of the order of:

$$\left(\frac{\mathrm{d}\nu}{\mathrm{d}I}\right)_{\mathrm{EC}} = \frac{\left(\frac{\mathrm{d}\nu}{\mathrm{d}I}\right)_{\mathrm{QCL}}}{1+\frac{l_{\mathrm{EC}}}{l_{\mathrm{QCL}}}} \approx 0.097\left(\frac{\mathrm{d}\nu}{\mathrm{d}I}\right)_{\mathrm{QCL}} \tag{4}$$

This gives a value of $\sim 9.7 \times 10^{-4}\ \frac{\mathrm{cm}^{-1}}{\mathrm{mA}}$. However in a double cavity system these two comb filters interact with each other causing a frequency pulling effect. Because of this effect, the tuning rate for a selected mode in a double cavity system will show a somewhat higher tuning rate than the one calculated for EC only using (4). This is demonstrated in Fig. 6a, where the frequency tuning rate of the laser selected mode in the simulated system without any mode tracking is $\sim 0.00135\ \frac{\mathrm{cm}^{-1}}{\mathrm{mA}}$, which for the simulated conditions is $\sim 40\%$ higher than the value given by (4). The overall trend observed for the wavelength tuning between two successive QCL FP resonator mode hops is also affected by this phenomena due to the interaction with the grating spectral reflectance function and as a result shows a lower wavelength tuning rate of $0.0093\ \frac{\mathrm{cm}^{-1}}{\mathrm{mA}}$ than the one expected for the QCL FP modes. For the system with enabled mode tracking by the EC, where the EC cavity length is adjusted to equalize wavelength tuning rates for both QCL FP resonator modes and EC FP resonator modes, the tuning rate of the selected laser mode is equal to the applied $\left(\frac{\mathrm{d}\upsilon}{\mathrm{d}I}\right)_{\mathrm{QCL}} = 0.01\ \frac{\mathrm{cm}^{-1}}{\mathrm{mA}}$. This can be observed for both mode tracking simulations presented in Fig. 6b and d. In Fig. 6b it is apparent that without appropriate adjustment of the grating angle mode hops will occur. Primarily, mode hops between adjacent QCL FP modes can be observed, which is indicated in Fig. 6b. However, for certain specific configurations of the three element wavelength selective filter (two cavities and the grating) a mode hop can also occur between two neighboring EC FP resonator modes. Such an effect is also depicted in Fig. 6b.

In a situation where only the grating angle is adjusted to track the laser frequency scan caused by scanning the laser driver current, mode hopping on the EC FP resonator modes will be observed. This is shown in Fig. 6c. By analogy to the simulation in Fig. 6a, the frequency tuning rate between the mode hops is $\sim 0.00135\ \frac{\mathrm{cm}^{-1}}{\mathrm{mA}}$. However, application of the grating angle tracking caused the overall trend line observed for the wavelength tuning to match the initial value of $0.01\ \frac{\mathrm{cm}^{-1}}{\mathrm{mA}}$.

In all cases where mode hops occur, a rapid wavelength change is accompanied by modulation of the overall losses within the resonator, which can be observed as changes in the relative intensity plotted in Fig. 6a, b, and c. This also indicates that the modulation of an intensity of generated light will be observed. However, for precise analysis of the laser power behavior, which is not a goal of the present work, linear as well as non-linear processes associated with the laser amplification should be taken into account.

Complete mode tracking allows mode hop free frequency tuning over the entire range as presented in Fig. 6d. No modulation of intra-cavity intensity is also observed, which will result in stable optical power of the active laser.

3.2 *Demonstration of mode-hop free wavelength tracking*

The performance of the mode tracking system was evaluated experimentally. The dependence of the laser frequency upon the position and angle of the diffraction grating controlled by the PZT actuators and the motor was measured separately for each actuator. All measured

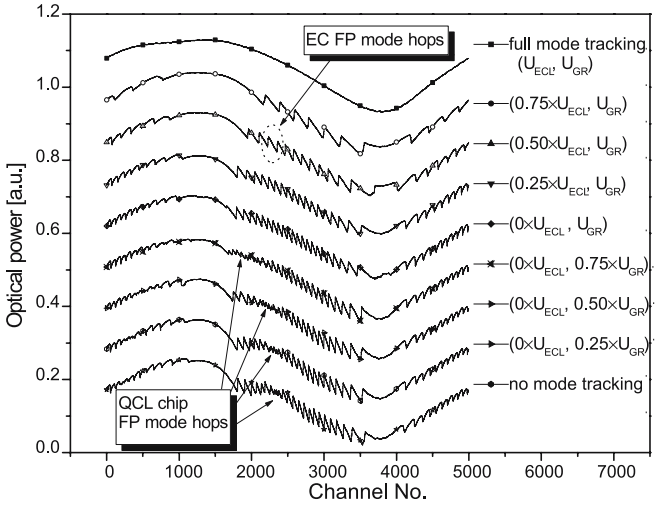

FIGURE 7 Demonstration of mode hop-free operation of the quantum cascade laser in an external cavity configuration using a PZT-actuated cavity mode tracking system

characteristics show high linearity with the coefficients of: $-0.0064\,\mathrm{cm}^{-1}$/unit for the motorized grating angle tuning, $0.049\,\mathrm{cm}^{-1}$/V (voltage applied to PZT actuator) for the PZT controlled grating angle tuning, and $0.036\,\mathrm{cm}^{-1}$/V for the PZT controlled EC length tuning. However, because of different factors such as PZT hysteresis, or translation stage mechanical backlash etc., the wavelength scan is usually optimized only in a single direction. This assures its good reproducibility and allows averaging of long scanning sequences.

To demonstrate an efficiency of the mode tracking system, the output optical power of the EC-QCL was monitored during an operation which involved applying different fractions of control signals U_{EC} and U_{GR} (for the EC length and for the grating angle respectively) required for full mode tracking. The laser was driven by ~ 630 mA current and modulated with arbitrary sinusoidal waveform. The results of this experiment are presented in Fig. 7, which shows successive laser power time series recorded for different amounts of the optimum laser mode frequency tracking. By analogy to the simulation above (see also Fig. 6), three of the discussed modes of operation can be observed with: no wavelength tracking (control signals U_{EC} and U_{GR} not applied), only grating wavelength tracking (only U_{GR} applied in full), and full wavelength tracking (both U_{EC} and U_{GR} applied in full). Both QCL FP resonator mode hops and EC FP resonator mode hops can be observed for partial mode tracking. Increase of the PZT control signals results in progressive separation of the mode hops, which finally leads to complete laser longitudinal mode tracking. Due to different kind of nonlinearities in the system such as PZT hysteresis or laser saturation the control voltages applied to the PZT mode tracking system must be set individually when operating conditions are varied.

3.3 *Wavelength tuning limitations*

The wavelength tuning properties in external cavity laser systems are usually limited by the mechanical properties of their architecture. The mechanical resonances of the system are also the main limiting parameters for the perform-

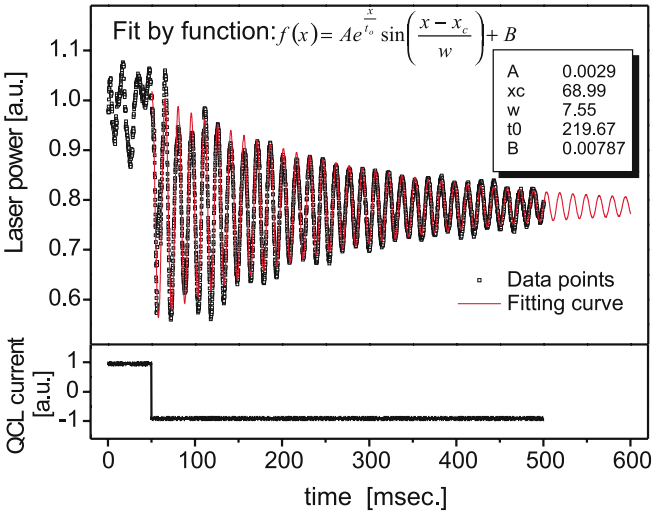

FIGURE 8 EC-QCL response measured with excitation by a step-like input signal

ance of wavelength scanning in the EC-QCL presented in this work. The wavelength scan in this system is controlled using a function generator, whose signal is used to modulate the QCL injection current and after appropriate conditioning of its amplitude and phase supplied as control signals to drive the PZT actuators of the EC-QCL. To determine the mechanical resonance frequency of the system, a rectangular waveform was applied to the input of the EC-QCL and the laser output was monitored. The response of the system is plotted in Fig. 8. Damped oscillations of the laser power are visible in the recorded photodetector signal as a result of mechanical vibrations excited in the EC laser system. The data points were fitted by a damped sinusoidal function. The frequency of these vibrations was determined to be $f_m = \sim 66$ Hz with a characteristic decay time of ~ 220 msec. The reported prototype system consists only of commercially available components. Consequently, the mass of the elements, which are a part of the EC manipulation system that must be actuated by the PZT, is relatively high and therefore such a low resonance frequency value was to be expected for this system. In order to suppress self-induced vibrations, the system should be driven by signals that do not excite any harmonics of the mechanical frequency. In this case, sinusoidal signals at frequencies lower than $f_m/10$ should provide optimum operating conditions and good performance of the laser.

The system response recorded for both a conventional triangular waveform and sinusoidal waveform scan (preferable for the present system) are illustrated in Fig. 9a and b, respectively. The applied parameters: peak-to-peak amplitude of $\sim 50\ \mathrm{mA_{p\text{-}p}}$ and frequency of 2 Hz were the same for both waveforms. From Fig. 8, it is clearly seen that the triangular signal due to rapid changes of the scan direction (the Fourier transform of such a signal contains high frequency harmonics) causes excitation of the gradually fading mechanical vibrations, which are not induced during sinusoidal scanning. Therefore, in all experiments performed with EC-QCL a sinusoidal wavelength modulation is applied.

4 Spectroscopic measurements

The wide wavelength tunability of the EC-QCL along with its suitability for high resolution spectroscopy are demonstrated by performing spectroscopic absorption measurements of nitric oxide, NO, and water, H_2O, at reduced pressures. The measured spectrum of a large section of the *P*-branch of the NO rovibrational spectrum between 1935 and 1961 $\mathrm{cm^{-1}}$, which could be accessed by the present EC-QCL is plotted together with a HITRAN 2000 simulation in Fig. 10. In this figure, successive spectral scans are recorded for different positions of the diffraction grating angle. Each scan is the average of 10 single 5000-points scans within 5 s. Thus a single high resolution spectrum containing spectral absorption data in range of $\geq 1\ \mathrm{cm^{-1}}$ can resolve spectral features separated by less than $0.006\ \mathrm{cm^{-1}}$ (see the inset of Fig. 10 depicting the NO $-R_{1/2}$ (23.5) line). All scans were performed using

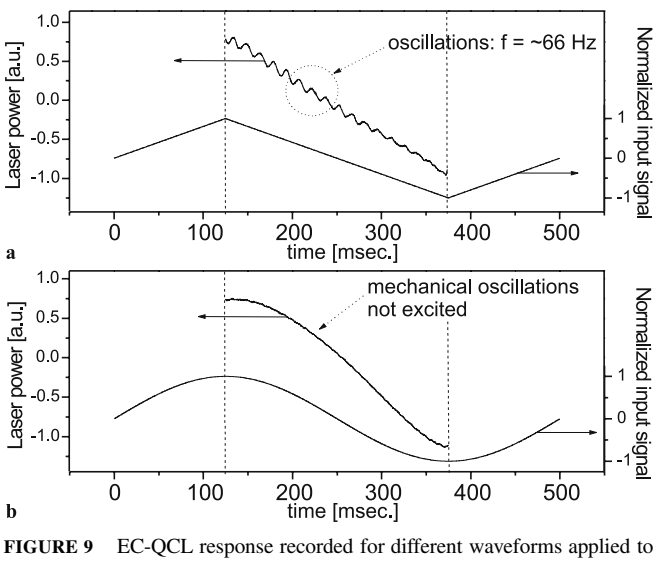

FIGURE 9 EC-QCL response recorded for different waveforms applied to modulate laser wavelength: (**a**) triangular waveform, (**b**) sinusoidal waveform

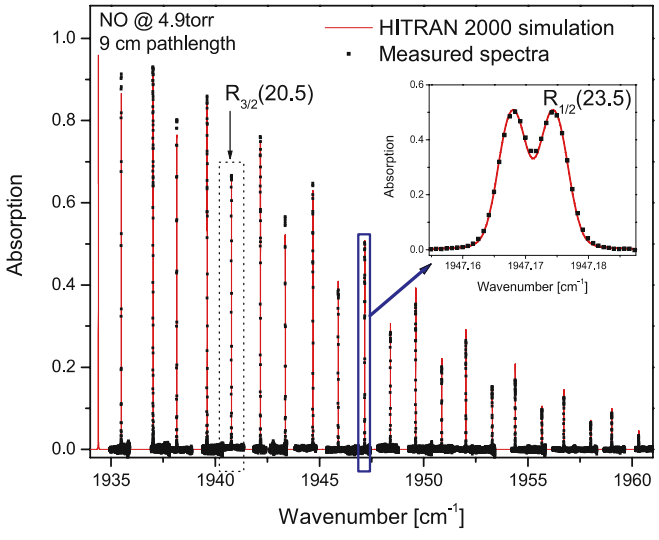

FIGURE 10 Nitric oxide absorption spectra measured at different diffraction grating angles of the external cavity quantum cascade laser. The narrow laser linewidth allows resolving two spectral peaks separated by $\sim 0.006\ \mathrm{cm^{-1}}$ (see *inset*)

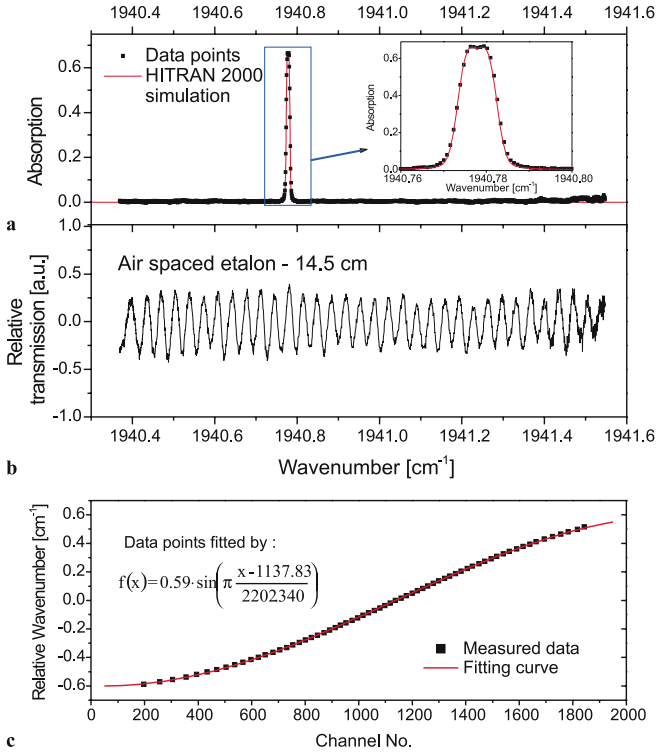

FIGURE 11 NO – $R_{3/2}$ (20.5) spectrum recorded within a range of a single scan of the EC-QCL

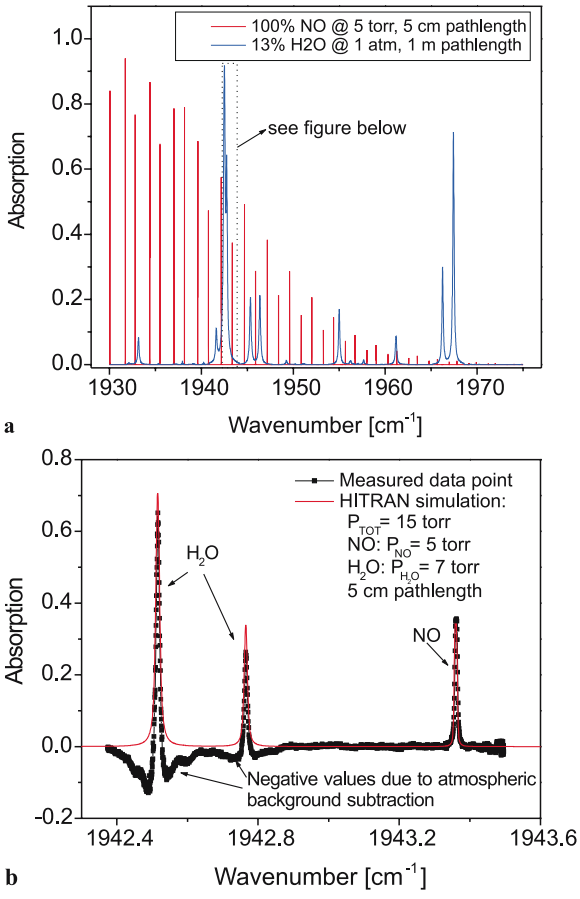

FIGURE 12 (**a**) Hitran simulated spectra of pure NO at 5 Torr in a 5 cm reference cell and ambient H_2O absorbing in 1 m open path of the laser beam. (**b**) Single spectral scan of NO and strong neighboring H_2O lines. Background measurement was performed with the reference gas cell removed from the beam path. Therefore, negative values of the calculated absorption spectrum are visible, which corresponds to reduced atmospheric water absorption (the negative part is related to a pressure broadened H_2O spectrum at atmospheric pressure)

sinusoidal modulation ($\sim 112\,mA_{p\text{-}p}$ at 2 Hz) of the laser current at an operating point of ~ 650 mA. For scan calibration an air-spaced low finesse etalon constructed of two ZnSe wedged windows separated by 14.5 cm was introduced into the beam path. A typical set of data recorded for a one of the component spectra presented in Fig. 10 is shown in Fig. 11. A wavelength calibrated spectra of NO $R_{3/2}$ (20.5) marked in Fig. 10 with a dotted box, along with the associated etalon fringe pattern and the calculated calibration curve are presented in the plots of Fig. 11a, b, and c, respectively. In this spectral region the separation of the component lines in NO $R_{3/2}$ doublets is much smaller than in the previously presented NO $R_{1/2}$ line. However, the fine spectral structure at the top of the line can still be resolved as shown in the Fig. 11a inset. Each single spectral scan was separately calibrated. The shape of the calibration curve presented in Fig. 11c is typical for all measured spectra. A fit of the calibration curve by the sinusoidal function confirms a linear relation between the laser current and frequency of the generated light with a tuning coefficient of $0.01\,\frac{cm^{-1}}{mA}$.

Within the tuning range of the EC-QCL several strong water absorption lines can be found. This is depicted in Fig. 12a, which shows the spectrum simulated using the HITRAN 2000 database for atmospheric H_2O and 1 m path length (this approximately corresponds to the open beam path in a real system) plotted together with the absorption of pure NO at 5 Torr and a 5 cm pathlength. The plot provides a spectroscopic "ruler", which allows a more precise wavelength measurement than the 1/8 wavelength monochromator used in the system (see Fig. 1). To demonstrate the capability of multi species concentration measurements within a single scan, a reference cell, which contained some residual H_2O, was evacuated for a short period of time and subsequently filled with pure NO (with a partial pressure of 5 Torr). The H_2O absorption lines at 1942.52 cm^{-1} and 1942.76 cm^{-1} were measured along with the NO–$R_{3/2}$ (21.5) line at 1943.36 cm^{-1}. The measured data together with a simulated spectrum is plotted in Fig. 12b. The simulation gives a partial pressure of H_2O of ~ 7 Torr. The background spectrum was measured with the reference cell removed from the optical path. This causes the effective path length in the atmosphere to increase by the reference cell length. The negative envelope around the water lines corresponds to an absorption spectrum of atmospheric H_2O within this additional pathlength. In the composite plot, the effects of pressure broadening and frequency shift are also observable.

5 Conclusions

A mode-hop free, widely tunable, continuous wave and thermoelectrically cooled EC-QCL capable of performing high resolution spectroscopic measurements has been developed and evaluated. The novel mode frequency tracking system is flexible and can be applied to other gain media at both shorter and longer wavelengths without modification of

its mechanical construction. The system provides independent wavelength tracking by all three wavelength-selective elements of the set-up (QCL cavity, EC, and diffraction grating), which makes it suitable for applications employing gain chips even with poorer efficiency AR coatings on the output facet. The current prototype instrument can provide a continuous mode-hop free fine frequency tuning range up to $\sim 2\,\mathrm{cm}^{-1}$ at $\lambda = \sim 5\,\mu\mathrm{m}$.

The overall spectrometer system performance was demonstrated by means of direct absorption spectroscopic measurements of NO and H_2O at reduced pressures. The main limitations in the scanning speed of the actual prototype system result from the vibrational resonances of the mechanical construction, which can be addressed in future EC QCL designs. Because the extended cavity mode spacing is much greater than the Doppler width, the present device demonstrates excellent suitability for spectroscopic trace gas concentration measurements using wavelength modulation techniques. This technique offers very high sensitivity and precision even with relatively slow scanning speeds. Its wavelength modulation capability combined with its wide tunability and high spectral resolution makes the EC QCL an excellent light source for a number of mid-IR spectroscopic applications such as trace gas detection.

ACKNOWLEDGEMENTS Financial support of the work performed by the Rice group was provided by the national aeronautics and space administration (NASA), the Texas advanced technology program, the Robert Welch foundation, and the Office of Naval Research via a subaward from Texas A&M university. The work performed at the University of Neuchatel, Switzerland was supported by the Swiss national science foundation NCCR "quantum photonics" as well as funding from the European project ANSWER.

REFERENCES

1 G. Wysocki, A.A. Kosterev, F.K. Tittel, Appl. Phys. B **4–5**, 617 (2005)
2 F.K. Tittel, D. Richter, A. Fried, Mid-Infrared Laser Applications in Spectroscopy, In: *Solid-State Mid-Infrared Laser Sources*, I.T. Sorokina, K.L. Vodopyanov (Eds.) (Springer Topics Appl. Phys. **89**, 445 2003)
3 D.D. Nelson, B. McManus, S. Urbanski, S. Herndon, M.S. Zahniser, Spectrochim. Acta A **60**, 3325 (2004)
4 J. Faist, C. Gmachl, F. Capasso, C. Sirtori, D.L. Sivco, J.N. Baillargeon, A.Y. Cho, Appl. Phys. Lett. **70**, 2670 (1997)
5 Q.V. Nguyen, R.W. Dibble, T. Day, Opt. Lett. **19**, 2134 (1994)
6 K.C. Harvey, C.J. Myatt, Opt. Lett. **16**, 910 (1991)
7 C.J. Hawthorn, K.P. Weber, R.E. Scholten, Rev. Sci. Instrum. **72**, 4477 (2001)
8 J.I. Vukusic, S.S. Rehman, Electron. Lett. **27**, 23 (1991)
9 G.P. Luo, C. Peng, H.Q. Le, S.S. Pei, W.Y. Hwang, B. Ishaug, J. Um, J.N. Baillargeon, C.H. Lin, Appl. Phys. Lett. **78**, 2834 (2001)
10 H.L. Zhang, C. Peng, A. Seetharaman, G.P. Luo, H.Q. Le, C. Gmachl, D.L. Sivco, A.Y. Cho, Appl. Phys. Lett. **86**, 111 112 (2005)
11 M. Beck, D. Hofstetter, T. Aellen, S. Blaser, J. Faist, U. Oesterle, E. Gini, J. Cryst. Growth **251**, 697 (2003)
12 S. Blaser, D.A. Yarekha, L. Hvozdara, Y. Bonetti, A. Muller, M. Giovannini, J. Faist, Appl. Phys. Lett. **86**, 041 109 (2005)
13 J.S. Yu, A. Evans, J. David, L. Doris, S. Slivken, M. Razeghi, IEEE Photon. Tech. Lett. **16**, 747 (2004)
14 J.S. Yu, A. Evans, S. Slivken, S.R. Darvish, M. Razeghi, IEEE Photon. Tech. Lett. **17**, 1154 (2005)
15 J. Faist, M. Beck, T. Aellen, E. Gini, Appl. Phys. Lett. **84**, 1659 (2004)
16 R. Maulini, M. Beck, J. Faist, E. Gini, Appl. Phys. Lett. **84**, 1659 (2004)
17 R. Maulini, D.A. Yarekha, J.M. Bulliard, M. Giovannini, J. Faist, E. Gini, submitted to Opt. Lett. (April 2005)
18 C. Peng, G. Luo, H.Q. Le, Appl. Opt. **42**, 4877 (2003)